SAND2022-16639C

Optical and Electrical Diagnostics of a High-Voltage Laser-Triggered Switch with Variable Impedance Load

Jacob A. Gottfried[1], Azer P. Yalin[2]
Colorado State University, Fort Collins, CO, 80523, USA

Charles E. Rose[3]
Sandia National Laboratory, Albuquerque NM. 87123

Mega-Volt class High-Voltage Laser-Triggered Switches (HV-LTSs) are often simulated using the Martin/Braginskii model with sufficient accuracy to be largely predictive. However, recently developed switches operating with low-inductance for nanosecond regime current pulses yield inconsistencies where the model both underpredicts rise times and overpredicts switch run time. The suspected reason for these inconsistencies lies in the model's assumptions, specifically, that the plasma conductivity is both spatially and temporally uniform. This study investigates HV-LTS plasma channel conductivity during the rising edge of the current pulse through both derivative (V-Dot) electrical probes and electron temperature measurements via laser Thomson scattering. A HV-LTS testbed utilizing an aqueous (variable impedance) resistive load was designed to produce experimental conditions similar to those found in larger pulsed power applications. This paper describes the design of the load and experimental results under a variety of load conditions and operating voltages of order 5 - 6 kV. Our results indicate the electron temperature increases during the rising edge of the current pulse suggesting that the plasma conductivity is temporally dependent. Further, electrical measurements show an increase in plasma conductivity during the rising edge of the current pulse. Evidence from both optical and electrical measurements calls into question the assumption of a temporally constant plasma conductivity in our experimental setup. Finally, we show that Spitzer's resistivity used by the Martin/Braginskii model does not accurately predict the measured plasma channel resistance.

I. Nomenclature

HV-LTS	=	High-Voltage Laser-Triggered Switch
TS	=	Thomson Scattering
T_e	=	Electron Temperature
n_e	=	Electron Density
σ	=	Plasma Conductivity
AVIL	=	Aqueous Variable Impedance Load
λ_D	=	Debye Radius
CVR	=	Current Viewing Resistor
Vdot	=	Derivative Voltage Probe

[1]Graduate student, Department of Mechanical Engineering. Member AIAA
[2]Professor, Department of Mechanical Engineering, Associate Fellow AIAA.
[3] Sandia National Laboratory, Member of Technical Staff

SAND2022-xxxx

II. Introduction

High-Voltage Spark-Gap switches are an essential component of pulsed power systems owing to their ability to deliver megampere currents and megavolt potentials on the order of milliseconds to nanoseconds. There are a variety of closure mechanisms used for spark-gap switches such as self-break [1], field distortion [2,3], and laser-triggering [4–7]; each having its own benefits and shortcomings. For example, High-Voltage Laser-Triggered Switches (HV-LTSs) are often utilized due to low temporal jitter, allowing for tens to possibly hundreds of HV-LTSs to be triggered at once [4,8–12]. HV-LTSs often sit between primary energy storage and the pulse forming network in large pulsed-power machines [13] facilitating both pulse compression and precise timing [14]. Primary energy storage is often arranged in a Marx bank (capacitive) configuration [15] to deliver large currents in short (microsecond) time spans. Switch closure is facilitated by an intense laser pulse focused at the center of the electrodes resulting in a plasma kernel [9]. This kernel expands for the duration of the laser pulse forming a plasma channel mid gap. Often the laser pulse width is shorter than the switch run time (Δt from laser pulse to meaningful current flow) and following a decrease in laser energy the plasma electron temperature and density are observed to temporarily decrease [16,17]. Given the plasma channel is conductive and mid gap, the externally applied electric field stress is dramatically increased such that streamers propagate connecting the electrodes resulting in a highly conductive path allowing meaningful current to flow [18].

Modern (low inductance) switch designs fail to be described by the Martin/Braginskii model [11]. This regime is highly sought after for pulsed power applications and has reinvigorated this area of research. Generally speaking, the Martin/Braginskii model is largely accurate for higher inductance switches commonly used [18–21]. Given the constant drive to reduce insertion losses (lower inductance is better) the need for a fundamental model that accurately describes the evolution of the plasma channel is apparent. The suspected reason for the observed discrepancy is the assumption that transient plasma properties are small by comparison and behavior is dominated by stable plasma characteristics, namely conductivity. Further, these plasmas are often described by Spitzer's conductivity which can be directly related to electron temperature and assumed constant [10,17,22]. Given these assumptions, it is clear to see why this model is largely accurate for higher inductance systems. Simply put, if the turn-on time is fast and on the order of the pulse width, transients matter and Martin/Braginskii, in its current form, is inaccurate.

This paper aims to discuss the development of an aqueous impedance matching resistor used to simulate a pulsed power load and investigate plasma channel characteristics during the rising edge of the current pulse in a HV-LTS. Laser Thomson Scattering (TS) is used to measure electron temperature and density of the plasma channel and derivative (non-contact) voltage monitors (V-Dot probes) are used to determine plasma conductivity through electrical measurements. The layout of the remainder of this paper is as follows: Section III. discusses the Martin/Braginskii switch model with its assumptions Section IV details the development of an aqueous variable impedance load for pulse power applications Section V presents the data analysis for the optical and electrical diagnostics Section VI presents the data analysis and discussion of the optical and electrical diagnostics. Finally, Section VII states the conclusions of this work.

III. The Martin/Braginskii Switch Model

The theory on the evolution of a plasma channel resistance in HV-LTS began with Braginskii's work to characterize the spark channel radial growth [20]. The fundamental result of Braginskii's work is the energy balance:

$$\frac{I}{\sigma} = 2\pi^2 \rho_0 (rr')^2 \xi \tag{1}$$

where I is *current*, σ is *plasma conductivity*, ρ_0 is *neutral gas density*, r and r' are *plasma radial growth and its first time derivative respectively*, and ξ is a *dimensionless constant* given by:

$$\xi = K_p \left[1 + \frac{2}{3(\gamma-1)}\right] \tag{2}$$

where K_p is the *coefficient of resistance* (assumed to be a constant = 0.9) [19], and γ is the *ratio of specific heats* (assumed =1.4 in dry room air). Developing this model, Braginkii solved for power balance arguing that a shock front is attached to the plasma channel during the rising edge and run time of the current pulse that then detaches when the current flow decreases [19,20]. Braginskii further used the analogy that this shock front acts as a piston, heating and

ionizing the working gas and creating a low-density (with respect to the working gas) plasma channel [20]. Fundamentally, the Braginskii model asserts that ohmic energy from the current passing through the plasma channel goes to enlarging the plasma channel, not heating it.

T. H. Martin used these results to develop theory regarding the energy losses in switches, resulting in a model of the temporal evolution of the plasma channel resistance that was shown to be accurate for several switch models [19]. Ultimately, his results are used in transmission line simulation programs for pulsed power systems, like BERTHA [11]. The Martin/Braginskii model gives the radius of the plasma channel at a point in time for a given current [19]:

$$r^2(t) = \left(\frac{4}{\pi^2 \rho_0 \xi \sigma}\right)^{\frac{1}{3}} \int_0^t I^{\frac{2}{3}} dt \tag{3}$$

where the conductivity of a plasma is calculated with a Spitzer-like conductivity model that is proportional to $T_e^{3/2}$ with minimal dependance on electron density [20]. Using Eqn. 3, the plasma channel resistance can be calculated as [19]:

$$R_{plasma} = \frac{L}{\sigma \pi r^2} \tag{4}$$

where L is the *spark gap length*.

In Eqn. 3, plasma conductivity is not considered to be a function of space or time. This, combined with the assertion that plasma conductivity is a function of T_e, results in any changes in electron temperature, either spatially or temporally, varying plasma conductivity. This would imply that Eqn. 3 may not contain all the necessary physics to model all types of HV-LTSs if changes in electron temperature are measured.

The above Martin/Braginskii model has worked for many switch versions that are designed to operate with microsecond to millisecond on-times [19,23]. However, the model has been found to have inconsistencies for new versions of switches designed for faster operation. In particular, the short on-times of new switches has led to the Martin/Braginskii model under predicting rise-times and over predicting the switch run times [11]. Recent research has shown that the electron temperature has both spatial and temporal dependencies during the decay phase of the plasma channel in a HV-LTS [17], motivating this study to develop an electrical diagnostic system working in tandem with laser Thomson scattering to investigate the plasma conductivity during the switch operation.

IV. Development of a Variable Impedance Load HV-LTS Testbed

A. HV-LTS Testbed

Figure 1 is the diagram for the switch testbed. The energy for the switch is provided a 20 nF, 100 kV capacitor with an equivalent series impedance of ~200 nH [22]. For each switch closure, the capacitor is charged by a 125 kV DC power supply (Glassman WK series PS/WK125P5.0-11). To protect the charging circuit from high voltage energy dumps in the case of accidental switch closure (self-break) during charging, a 20 kΩ copper sulfate (CuSO4) liquid charge resistor is used to connect the power supply to the energizing relay (Ross 40 kV-air). The relay connects the power supply to the capacitor during the charge cycle but leaves the switch and capacitor electrically isolated during the laser-triggered closure. To simulate a pulsed power test condition, the energy is dumped into a high-energy aqueous resistor, simulating an experimental load [22,24].

The HV-LTS for this study consists of two electrodes with a 3.5 mm gap. The switch has been modified to allow optical access on two axes (4 apertures) in addition to the laser triggering access. This allows for the plasma to be probed with a laser and have the scattered photons collected at 90 degrees. In addition to optical access, there is also a port to allow gas to flow into the switch. For the current study, this port supplies a purge flow of Ultra Zero Air during the charge cycle, resulting in ambient pressure and temperature conditions. The switch is triggered by a single 14 mJ, 12 ns FWHM pulse from the 1064 nm output of a Nd:YAG laser (Quantel Big Sky). The laser beam is steered to the height of the switch using two laser line turning mirrors (see Fig. 4 for optical layout). In addition to optical access, the HV-LTS testbed is equipped with two derivative coupled non-contact voltage monitors (V-Dot probes) positioned 5 mm from the switch's positive and negative electrodes in the radial direction as depicted in Fig. 1.

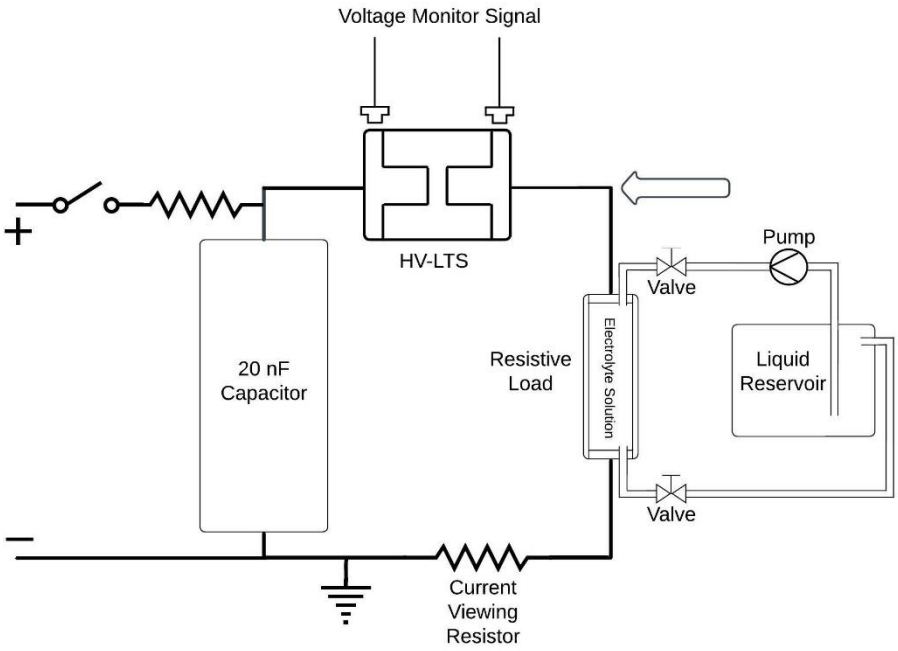

Fig. 1 HV-LTS testbed diagram.

B. Design for an Aqueous Variable Impedance Load

Past iterations of a HV-LTS testbed used a short-circuit electrical system. This resulted in significant reflection in current during switch operation [10,17]. Although this provided similar physics during the rising edge of the current pulse, it does not provide an accurate representation of a pulse power load. To emulate a proper pulsed power load, an aqueous variable impedance load (AVIL) has been designed. Figure 1 depicts the full liquid exchange loop used for tuning the impedance of the load. This includes the AVIL, a diaphragm pump, valves, and a liquid reservoir. The geometry of the aqueous load was designed to have similar dimensions as the capacitor allowing for a compact circuit, minimizing circuit transmission losses and transmission line charge storage. Figure 2a is a representation of the physical electrical circuit and Fig 2b. is a drawing of the AVIL cross section. At the center of each stainless-steel electrode is a ¼ - 20 tapped hole to allow a copper electrical transmission bracket to be attached. In addition to this, there is a port with a threaded connector to allow the liquid processing loop to be connected. To impedance match the switch, the resistor must be accurately tunable below 10 Ω. For ease of use, the internal geometry is designed to use a simple aqueous solution of table salt (NaCl) in distilled water as the electrolyte. The result is an AVIL that is tunable between 2 - 100 Ω where the upper bound is determined by the purity of water used (and possible corrosion of the electrodes).

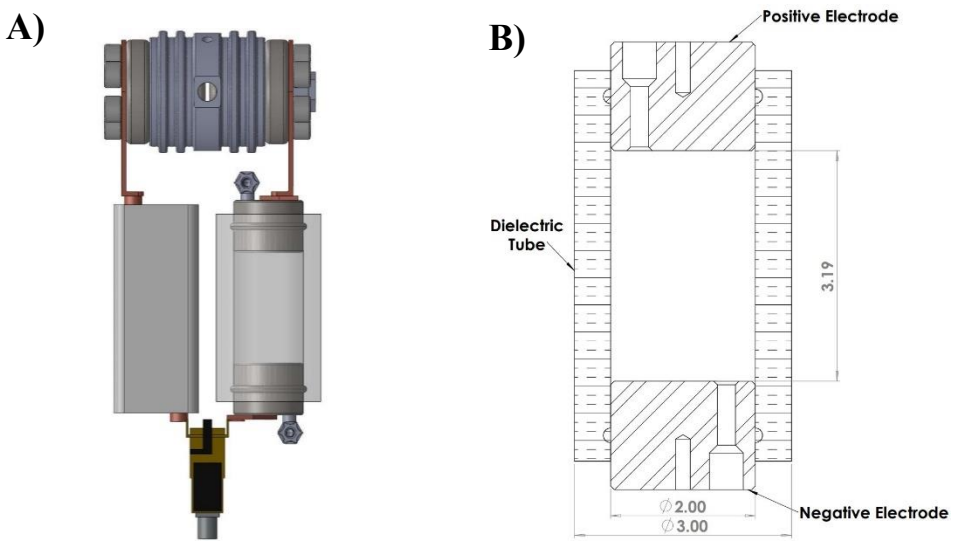

Figure 2 A) Physical design of the electric circuit. B) Drawing of the AVIL.

To further improve the tunable accuracy of the AVIL, a liquid exchange loop and reservoir are used. The larger volume of water lowers the sensitivity of added salt mass to the solution concentration allowing for easy fine impedance tuning. Furthermore, the liquid exchange loop allows for *in situ* changes to the impedance allowing the AVIL to be impedance matched to the circuit without the need to measure the exact resistance. During the operation and data collection, the pump is turned off and the valves are sealed to minimize changes in impedance. The result of this AVIL design is a HV-LTS testbed with fine control of the load impedance. Figure 3A is data of the current trace, as measured by the current viewing resistor (CVR, T&M Research Products W-2-001-6FC), for cases of the original short-circuit current, matched impedance, overdamped, and underdamped load for a 6 kV charged capacitor. Where time zero is referenced to the time of the triggering laser pulse (as determined by a 10% rise in a photodiode 1 in Fig. 4).

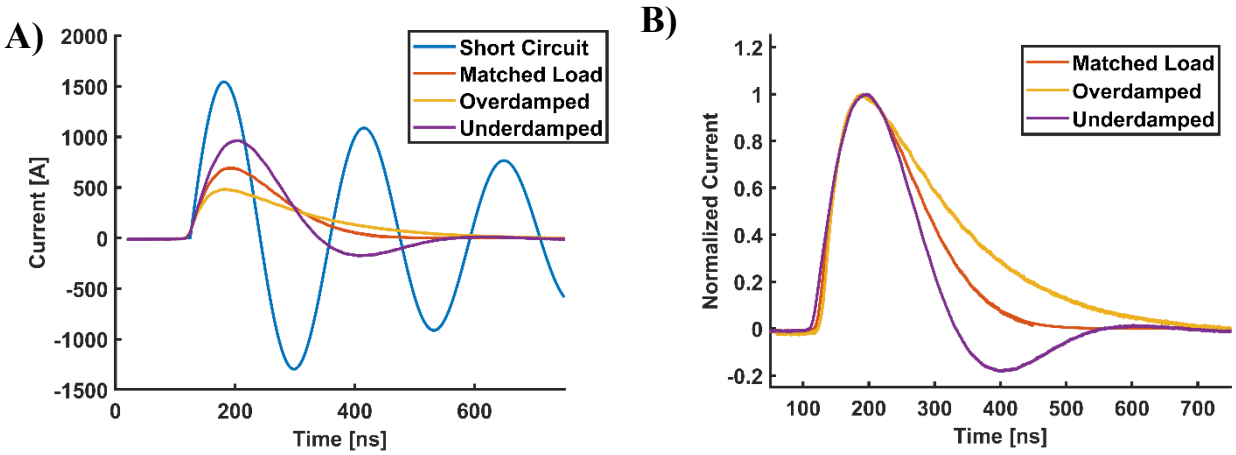

Figure 3 A) Comparison of circuit current based on load impedance matching. B) Normalized current trace for circuits using a load.

Figure 3B are the same current traces as Fig. 3A, normalized to the peak value. From the comparison of normalized current traces, it is seen that the characteristic rise time and general trend of the current pulse rising edge is not affected by the load. During the rising edge of the current pulse, the electrical characteristics are dominated by the pulse forming network.

V. Experimental Methods and Data Analysis

A. Laser Thomson Scattering

This work utilizes laser Thomson Scattering (TS) to measure the electron temperature and density of the plasma channel during the HV-LTS switch operation. TS has been shown to accurately measure the electron temperature and density of plasmas under a variety of conditions including fusion reactors [25], laser induced plasmas [16,26], nanosecond pulsed discharges [27], and within the plasma channel of a HV-LTS [17,22] all without any assumptions regarding plasma conditions [28]. For the plasma conditions in this work, the electron temperatures and densities result in a class of TS referred to as collective Thomson scattering. Collective Thomson scattering is the Doppler shifting of incident photons due to interactions with charged particles within the plasma (mostly electrons due to their low mass). This scattering takes place over an optical wavelength much smaller than the Debye radius of the plasma and therefore photons only interacts with shielded electrons [29–31]. This results in a TS spectrum with two distinct satellite peaks symmetrically separated from incident lasers wavelength (due to scattering from electrons) along with two satellite peaks due to the ions. However, the ion contributions are spectrally close to the incident lasers wavelength leading to difficulties spectrally resolving the feature from other forms of scattering at the laser's wavelength [16]. This work focuses on the electron satellite peaks alone.

Figure 4 is the optical setup for TS which consists of a probe laser using a frequency doubled Nd:YAG (Quantel Q-Smart 100) operating at 532 nm with a pulse energy of 28 mJ and duration 8 ns (FWHM). The beam is weakly focused by a 400 mm focal length plano-convex lens such that the waist is at an iris upstream of the switch. The iris removes divergent light and reduces elastic scattering off the switch electrodes. After the iris, the probe beam expands to a diameter of ~ 0.9 mm in the region of interaction with the plasma channel. The scattered light, along with the plasma luminous emission, is collected by a 150 mm focal length plano-convex lens at 90 degrees. In the collection path, a 532 nm Bragg Notch Filter with a 0.1 nm FWHM is used to reduce Raleigh and elastically scattered laser by an optical density of approximately 3-4 to avoid saturating the ICCD or distorting the TS spectrum. After the Bragg Notch Filter, the collected light is one-to-one imaged onto the 40 μm slit of a spectrometer (Princeton Instruments SP-2300i) where it is dispersed with a 1200 groove/mm grating onto the ICCD (Princeton Instruments PI-MAX4) using a gate width of 10 ns. This results in a spectral resolution and wavelength range of 0.030 and 30 nm respectively.

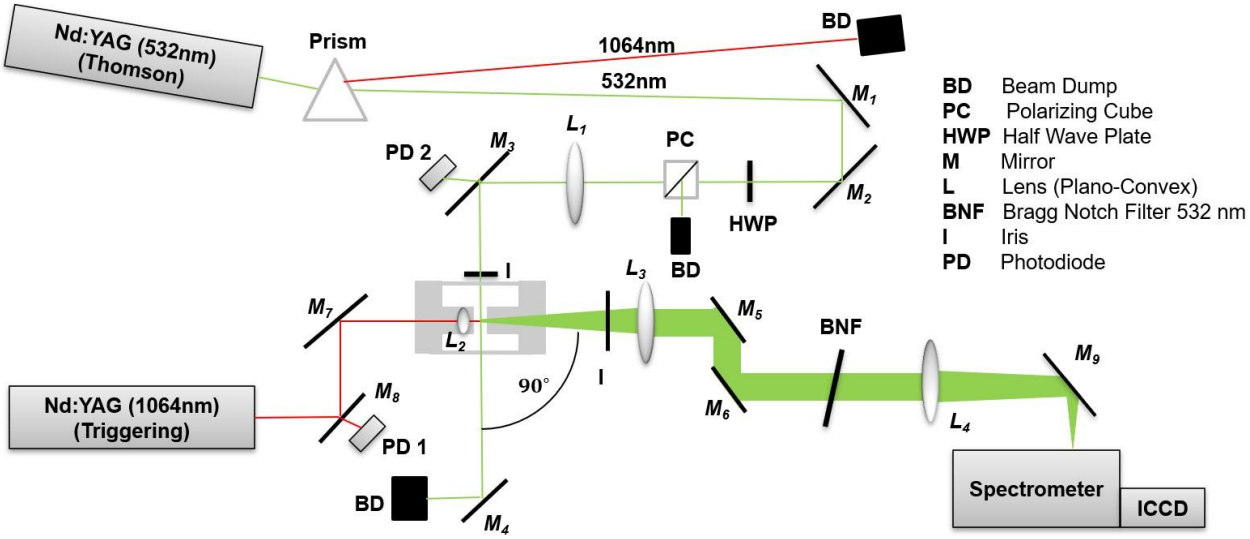

Figure 4 Optical layout used for laser Thomson scattering.

Thomson scattering has a small scattering cross section resulting a signal much smaller than the plasma luminous emission. To improve the signal, accumulations of many switch closures are required. For delay times earlier than 500 ns (current flow is between ~120 ns and 450 ns) , the plasma emission is much stronger than the TS signal (up to 100 times more) and therefor, spectra from 200 switch closure events are needed for a sufficient signal-to-noise. In addition to the stronger plasma emission, the electron temperature and densities present at delay times earlier than 350 ns result in a wavelength separation of the electron satellite peaks that is greater than the ICCD wavelength range, requiring

fitting to a single peak [26]. These concerns combine to result in an error for the electron temperature and density to be ~ 20%.

To determine the electron temperature and density of the experimental TS spectrum, a simulated TS spectrum is calculated based on guess values for electron temperature and density. The simulated TS spectrum is fit to the experimental TS spectrum (after subtracting the plasma emission background recorded under the same conditions) via a least-squares minimization method. To simulate the TS spectrum the Salpeter approximation in the following form is used [22,32–34]:

$$S(\boldsymbol{k},\omega) \approx \frac{\sqrt{2\pi}}{\nu_{te}}\Gamma_{\alpha}(\xi_e) \tag{5}$$

where Γ_{α} is the *line shape function* and ξ_e is the *ratio of phase velocity of the wave to the electron thermal velocity* [35] and ν_{te} is the *electron thermal velocity*. To further improve the accuracy of the TS simulated spectra, a calibration based on spontaneous rotational Raman scattering is performed [17]. Figure 5 is an example of a TS spectrum and fitted simulation.

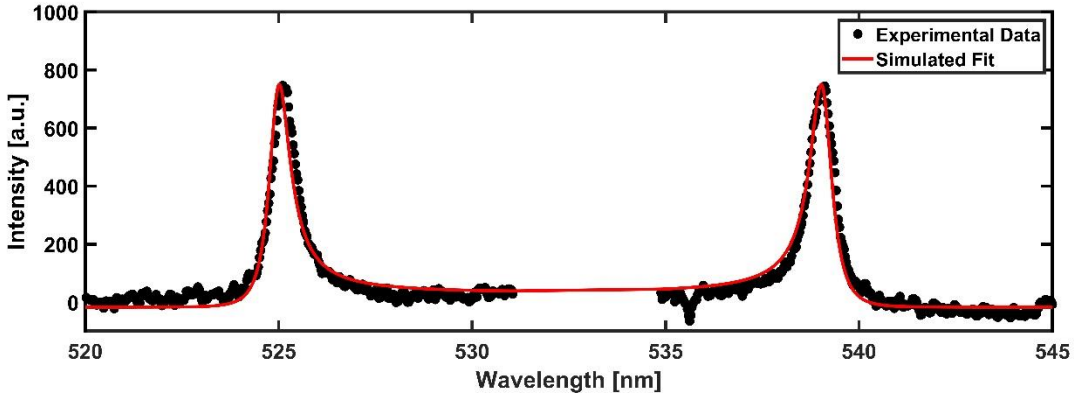

Figure 5 Simulated Thomson scattering spectrum fit to experimental spectrum recorded 1 μs after a 6 kV pulse. The fit resulted in a T_e of 3.5 eV and a n_e of 3.5x10^{17} cm^{-3}

B. Electrode Voltage Measurements with V-Dot Probes

V-Dot probes are a capacitive voltage monitor that responds to changes in the electric field and therefore produce a derivative response, an invaluable diagnostic tool for pulsed power applications. When compared to traditional contact resistive voltage monitors, V-Dot probes have three major advantages. Firstly, V-Dot probes are non-contact allowing for essentially non-perturbative measurement. For example, in this work it was found that recording the positive electrode's voltage with a resistive monitor (Tektronix P6015A) during the charge and isolate portions of the switch operation lead to significant current through the monitor that altered switch triggering characteristics. Secondly V-Dot probes offer high bandwidth coupling generally limited by the oscilloscope used to record data. Given these monitors produce a differential signal, either numerical or analog integration is required with their own bandwidth considerations. Finally, V-Dot probes don't suffer from a resistive voltage coefficient allowing for measurement of up to megavolt potentials where resistive monitors are infeasible.

1. Analog RC Integration

Due to the derivative nature of V-Dot probes, one needs to integrate the signal to determine the change in voltage. Integration can either be done through direct numerical methods or with an analog RC integrator. Direct numerical integration is the easiest route, however, due to the derivative response, signals often have high frequency information that can be aliased by low cutoff frequency oscilloscopes. Should aliasing occur error in numerical integration will result in erroneous data. As there is no way to know if aliasing is occurring without knowing the original signal, the only solution is to use a high sample rate (expensive) oscilloscope. Alternatively, one can use an analog RC integrator, lowering the oscilloscope sample rate requirements with minimal loss of high frequency information assuming a high-

performance RC integrator was used. For the work in this paper, we chose to use analog integration due to the lower equipment requirements. Although analog integration requires less expensive recording equipment, the capacitive nature of the RC integrator results in an inability to transmit DC voltages. Further, the nature of the RC integrator also results in an associated voltage droop in the output signal. Equation 6 is used to correct for integrator voltage droop based on empirically measured RC time constant, τ [36].

$$S(t)_{corrected} = S(t) + \frac{3}{2\tau}\int_{t_{start}}^{t} S(t')\,dt' \tag{6}$$

where S(t) is the *measured output voltage*. The integrators used for this work have a time constant of ~ 1 μs, five times longer than the measured voltage signal. Figure 6 is an example of this calibration performed on the integrated V-Dot signal for the negative electrode during switch closure.

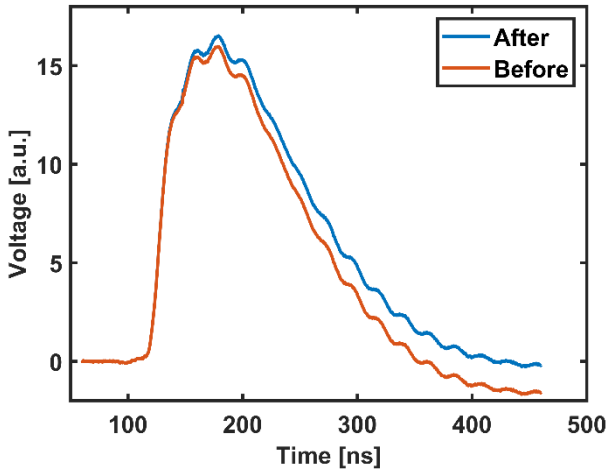

Figure 6 Voltage droop correction on negative electrode V-Dot probe signal for a switch closure at 120 ns.

2. V-Dot Probe Calibration

V-Dot probes respond to changes in the electric field and therefore their output depends heavily on their position in an electric field requiring the signal output to be calibrated *in situ*. For this paper, calibration was performed by measuring 200 signal traces with a calibrated resistive voltage monitor (Tektronix P6015A) attached to an electrode and 200 signal traces (due to the same switch closure events) with a V-Dot probe using an analog integrator on an oscilloscope (Tektronix TDS5034B). For improved accuracy, the 200 traces are averaged. The droop corrected V-Dot signal is fit to the resistive voltage monitor signal with a linear transformation and the best fit is determined by a cost function minimization of the residual sum of squares for the two signals. The error in fit coefficients was determined using the root mean square of the resistive voltage monitor error, oscilloscope error, and statistical variance of the 200 shot averages.

VI. Results and Discussion

A. Optical Diagnostics

1. Laser Thomson Scattering

Laser Thomson scattering measurements of the electron temperature (T_e) and density (n_e) within the plasma channel of the HV-LTS under two operating conditions were recorded. In case one, the capacitor was charged to 6 kV and in case two, the capacitor was charged to 5 kV. For both cases, the AVIL was not changed resulting in a matched load condition for case one and a slightly underdamped load for case two. Figure 7A are the results for T_e vs time for the two cases. In both cases, the triggering laser forms an initial plasma at a delay time of zero which then decays until

120 ns at which point the switch closes, current transfer initiates and the plasma is heated. For both cases, the initial laser-induced plasma decays to a temperature of ~ 8 ± 1.6 eV at the time of switch closure. This value is similar to the decay trends of atmospheric pressure laser-induced air plasmas in literature [16]. During the rising edge of the current pulse (120 ns - ~200 ns), both cases see a rise in electron temperature at a similar rate to a maximum temperature of ~26 ± 5 eV. These results directly contradict the assumed conditions of the Martin/Braginskii model (constant T_e) during the rising edge current flow. The suspected reason for this is the highly transient nature of the switch operation. Since the current flow does not stabilize (rise time is the same order of magnitude as on time), the physics assumed in the Martin/Braginskii model power balance may not apply and therefore, Joule heating raises the plasma temperature. Following the peak current flow, the electron temperature decays at a rate proportional to $t^{-1.48}$ for ~ 1.5 µs following the current pulse.

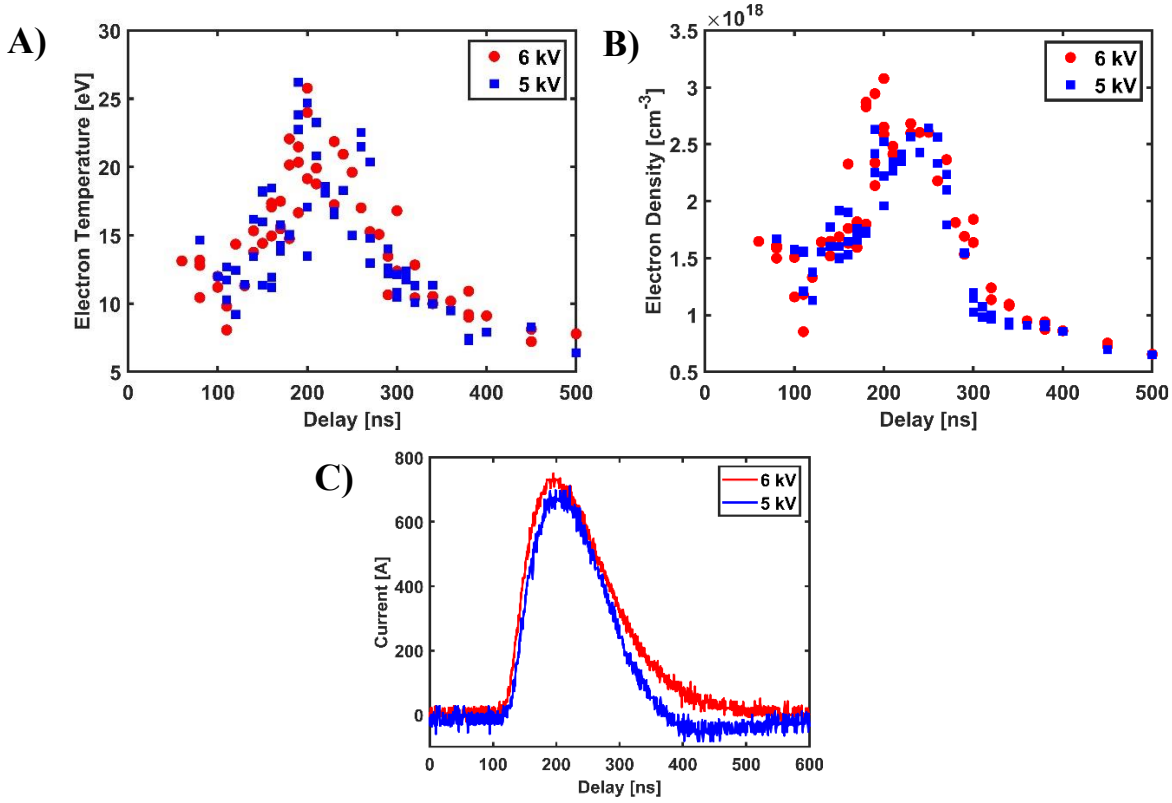

Figure 7 Thomson Scattering results of A) electron temperature and B) electron density within the plasma channel of HV-LTS along with the C) associated current trace. Data represents a single load configuration resulting in a matched and underdamped condition for a 5 and 6 kV charge case respectively. Error for the electron temperature and density are of ~20% of the measured value.

Figure 7B) is the electron density during the current pulse. As with the electron temperature, the initial laser-induced plasma decays to a value of ~ 1 ± 0.2 x 10^{18} cm^{-3} at a delay time of 120 ns, a value comparable to similar laser-induced air plasma decays in literature [16]. During the rising edge of the current pulse, both cases see a similar rise in electron temperature to a maximum of ~ 2.5 ± 0.5 x10^{18} cm^{-3} at a delay time of ~ 250 ns, a time ~ 20 ns following the peak in the current pulse, Fig. 7C. During the falling edge of the current pulse, the 5 kV charge case with an underdamped load has a sharp decrease in electron temperature until a delay time of 300 ns where it levels off before decreasing again at 400 ns. The 6 kV charge case with a matched load has a slower measured decrease in n_e and does not exhibit a period of leveling off in the decay. Both trends seem to match with the current flow in the system for their respective case, however, these differences are well within the ± 20% measurement error. At delay times greater than 400 ns, both cases reach similar electron densities and both decay at a rate proportional to $t^{-1.64}$ for 2 µs following the end of current flow.

2. Plasma Channel Radial Growth

In addition to Thomson scattering, the radial growth of the plasma channel during the current pulse of the 6 kV matched load case was measured. This was accomplished by recording full-chip ICCD images where the spatial dimension (radial dimension of the plasma channel) is preserved. From the ICCD images, the plasma channel diameter was determined by recording the number of pixels (in the radial direction) above a detection threshold and converted to distance using the imaging ratio and physical pixel size. From this, it was found that the plasma channel expands according to the power law relationship :

$$r\,[mm] = 0.0128t^{0.6259 \pm 0.017} \tag{7}$$

This matches rate of plasma channel expansion for a variety of high-voltage spark-gap switches operating under a variety of conditions in literature [9,10,19] as well as the trend assumed in the Martin/Braginskii model [19,20].

B. Electrical Diagnostics

Using the calibrated V-Dot probes, the voltage of both the positive and negative electrodes was recorded during switch operation. Several load conditions were tested with the capacitor charged to a constant 6 kV including an underdamped (~4 Ω), overdamped (~10 Ω), and matched (~6 Ω) impedance load case. For each case, 200 single switch events were recorded and averaged to reduce noise. Figure 8 A-C are the voltages present on each electrode for each load case.

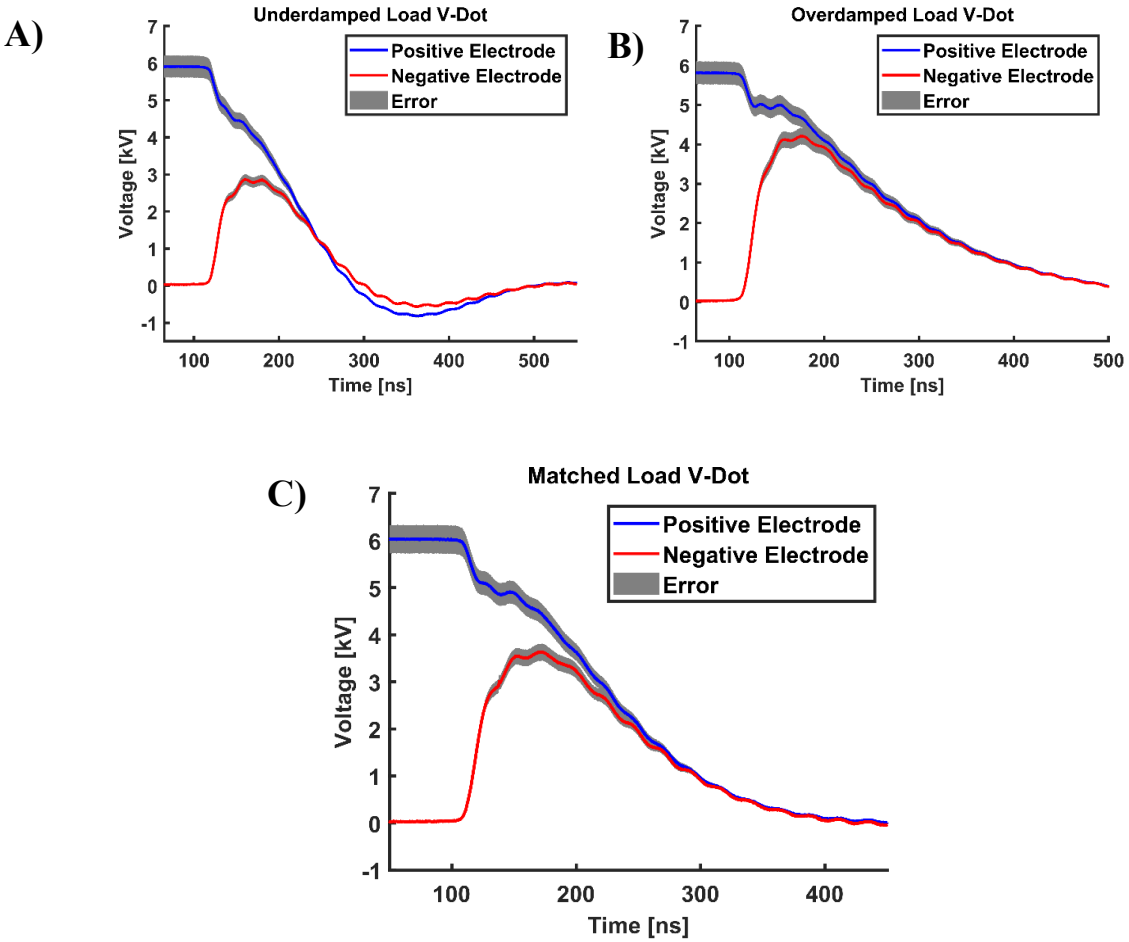

Figure 8 Calibrated V-Dot signals for corresponding to a 6 kV capacitor charge with a A) underdamped load, B) an overdamped load, and C) a matched load.

From the voltage signals present in Fig. 8, the voltage drop across the plasma channel is calculated. The voltage drop is used in combination with the currents measured with the CVR in Fig. 3A to calculate the plasma channel impedance according to Ohm's law:

$$R_{plasma} = \frac{V_{drop}}{I} \tag{8}$$

Figure 9A is the impedance of the plasma channel, calculated by Eqn. 8, plotted against the delay time for the underdamped, overdamped, and matched load case. In all cases, the capacitor was charged to 6 kV resulting in the same pulse forming network configuration for each case. As with the rising edge of the current, it is expected that the impedance collapse during the rising edge will be determined solely by the driving pulse forming network (capacitor in this case). The measured impedance collapse does follow this trend with minimal difference in the impedance collapse for different load cases.

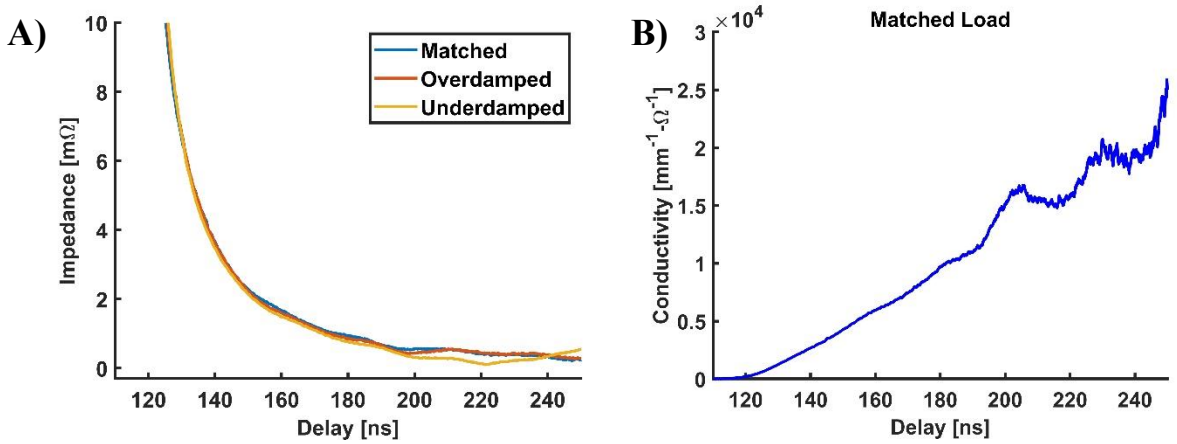

Figure 9 A) Impedance collapse comparison for an underdamped, overdamped, and matched load case where the driving pulse forming network configuration remains the same. B) Conductivity calculated using Eqn. 4 for the matched load case.

Using the values for impedance calculated with Eqn. 8 and the plasma channel radius calculated with Eqn. 7, Eqn. 4 can be used to calculate the conductivity of the plasma channel which is plotted in Fig. 9B. We found that for the conditions and switch studied, the plasma channel conductivity is linearly increasing during the rising edge of the current pulse. This directly contradicts the assumption used to derive the Martin/Braginskii model (Eqn. 3) that stated the system will be dominated by a spatially and temporally constant plasma conductivity.

C. Comparison of Optical and Electrical Diagnostics

In the original work by Braginskii, the plasma conductivity was assumed to be a function of electron density following the Spitzer like plasma resistivity model [19,20,37,38]:

$$\eta = \frac{2\sqrt{2\pi}}{3}\frac{Ze^2\sqrt{m_e}\ln\Lambda}{(4\pi\varepsilon_0)^2(k_BT_e)^{3/2}} = \frac{1}{\sigma} \tag{9}$$

where Z is the *degree of ionization*, e and m_e are the *elemental charge and mass*, ε_0 is the *electric permittivity*, k_B is the *Boltzmann constant*, and Λ is the *Coulomb logarithm* defined by [39,40] :

$$\ln\Lambda = \frac{\lambda_D}{r_\perp} = 12\pi n_e\lambda_D^3 \tag{10}$$

where λ_D is the *Debye radius* of the plasma and $r_\perp$ is the *minimum radius of the Coulomb collision*. Using the data from Fig. 7A and 7B for the 6 kV matched load case, the plasma resistivity is calculated based on Eqns. 9-10. Continuing, the impedance of the plasma channel is calculated according to [19]:

$$R = \frac{\eta L}{\pi r^2} \tag{11}$$

where L is the *length of the plasma channel* (spark gap distance, in this case) and r is the e*xperimentally determined plasma channel radius* as determined by Eqn. 7.

Figure 10 is the comparison of plasma channel impedance collapse calculated from electrical measurements through Ohm's law and by optical measurements using the Spitzer resistivity model. The Spitzer resistivity model predicts a similar trend for the impedance collapse. However, the predicted resistance is two orders of magnitude greater than the measured impedance. This could be the result of incorrect Thomson scattering measurements; however, this is unlikely due to the order of magnitude for the error required to reconcile the difference. The more likely cause is that the Spitzer resistivity does not correctly model the physics present during the rising edge of the current pulse. For example, the Spitzer resistivity was derived for fully ionized plasma assuming all momentum transfer is from electrons to ions in far range Coulomb collisions [37,41–43]. The plasma investigated in this paper has a maximum ionization fraction of ~0.1 (as determined by the difference between the number density of ambient air and recorded electron density, assuming a singly ionized plasma). At a 0.1 ionization fraction, it is likely that the electron-neutral, ion-neutral, and neutral-neutral collisions cannot be ignored as a source of momentum transfer.

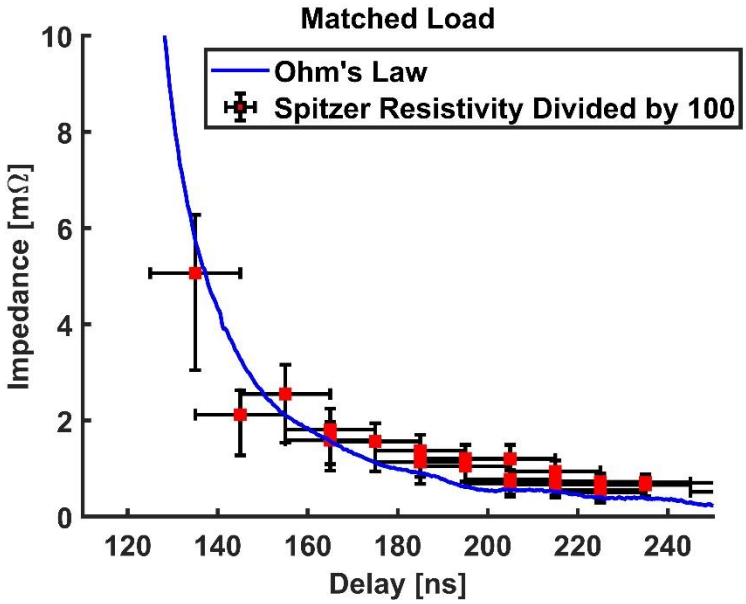

Figure 10 Comparison of plasma channel impedance calculated from electrical measurements (Ohm's law) and Optical measurements (Spitzer Resistivity) for the 6 kV matched load case.

VII. Conclusion

The Martin/Braginskii model is widely used to simulate the operation of HV-LTSs. The model assumes a temporally constant plasma conductivity. To calculate the plasma conductivity, the Spitzer's resistivity model is used and therefore the plasma conductivity is directly proportional to the electron temperature. This work has investigated the electron temperature during the current pulse via the laser Thomson scattering diagnostic. The measured result is that, for the switch and test conditions used, the electron temperature rises during the current pulse without stabilizing, directly contradicting the assumption of a temporally constant plasma conductivity. In addition to the optical measurements, the plasma conductivity was determined through electrical measurements using non-contact V-Dot

probes. From the electrical measurements it was calculated that the plasma conductivity linearly increases during the rising edge of the current pulse. This further indicates that the assumption of the temporally constant plasma conductivity is not valid for HV-LTSs operating in a transient dominated regime. In addition to the changing plasma conductivity, the Spitzer resistivity model does not accurately predict the plasma channel resistivity for the conditions tested in this paper. The likely cause of the overestimation for resistance by the Spitzer resistivity model is due to the low (incomplete) ionization level of the studied switch plasma channel.

In conclusion, HV-LTSs operating in a regime dominated transient effects in the current pulse (switch turn-on-time is same order of magnitude as pulse width) may not be accurately modeled with the Martin/Braginskii model due to a non-temporally constant plasma conductivity. Future work will be conducted at a range of operating conditions to determine if this discrepancy between the Martin/Braginskii model assumptions and measured switch operation is very specific to our switch operating conditions or rather if it is indicative or a broader gap within the model.

Acknowledgements

Colorado State University acknowledges funding support from Sandia National Laboratories. Sandia National Laboratories is a multi-mission laboratory managed and operated by National Technology & Engineering Solutions of Sandia, LLC, a wholly owned subsidiary of Honeywell International, Inc., for the U.S. Department of Energy's National Nuclear Security Administration under contract DE-NA0003525. This paper describes objective technical results and analysis. Any subjective views or opinions that might be expressed in the paper do not necessarily represent the views of the U.S. Department of Energy or the United States Government.

We would also like to acknowledge funding support from the National Science Foundation Division of Physics Award 2010466.

References

[1] Lehr, J. M., Abdalla, M. D., Burger, J. W., Elizondo, J. M., Fockler, J., Gruner, F., Skipper, M. C., Smith, I. D., and Prather, W. D. Design and Development of a 1 MV, Compact, Self Break Switch for High Repetition Rate Operation. In *12th International Pulsed Power Conference*, No. 2, Monterey, CA, USA, 1999, pp. 1199–1202.

[2] Song, F., Li, F., Zhang, B., Zhu, M., Li, C., Wang, G., Gong, H., Gan, Y., Jin, X., Novac, B. M., and Smith, I. R. "A Compact and Repetitively Triggered, Field-Distortion Low-Jitter Spark-Gap Switch." *IEEE Transactions on Plasma Science*, Vol. 47, No. 8, 2019, pp. 4105–4113. https://doi.org/10.1109/TPS.2019.2926617.

[3] Pashaie, B., Schaefer, G., Schoenbach, K. H., and Williams, P. F. "Field-enhancement Calculations for a Field-distortion Triggered Spark Gap." *Journal of Applied Physics*, Vol. 61, No. 2, 1987, pp. 790–792. https://doi.org/10.1063/1.338182.

[4] Guenther, A. H., and Bettis, J. R. "The Laser Triggering of High-Voltage Switches." *Journal of Physics D: Applied Physics*, Vol. 11, No. 12, 1978, pp. 1577–1613. https://doi.org/10.1088/0022-3727/11/12/001.

[5] Woodworth, J. R., Frost, C. A., and Green, T. A. "Uv Laser Triggering of High-voltage Gas Switches." *J. Appl. Phys.*, Vol. 53, 1982, p. 7.

[6] Kushner, M. J., Kimura, W. D., and Byron, S. R. "Arc Resistance of Laser-triggered Spark Gaps." *Journal of Applied Physics*, Vol. 58, No. 5, 1985, pp. 1744–1751. https://doi.org/10.1063/1.336023.

[7] Pendleton, W. K., and Guenther, A. H. "Investigation of a Laser Triggered Spark Gap." *Review of Scientific Instruments*, Vol. 36, No. 11, 1965, pp. 1546–1550. https://doi.org/10.1063/1.1719388.

[8] Larsson, A., Yap, D., Au, J., and Carlsson, T. E. "Laser Triggering of Spark Gap Switches." *IEEE Transactions on Plasma Science*, Vol. 42, No. 10, 2014, pp. 2943–2947. https://doi.org/10.1109/TPS.2013.2297161.

[9] Wolford, M. F., Myers, M. C., Hegeler, F., and Sethian, J. D. "Dynamics of Laser Triggered, Gas-Insulated Spark Gaps During Repetitive Operation." *IEEE Transactions on Plasma Science*, Vol. 44, No. 10, 2016, pp. 2410–2423. https://doi.org/10.1109/TPS.2016.2606249.

[10] Rose, C. E. "DEVELOPMENT OF A HIGH-VOLTAGE LASER TRIGGERED SWITCH FACILITY INCLUDING INITIAL OPTICAL AND ELECTRICAL DIAGNOSTICS." *M.Sc. Thesis, Mechanical Engineering Dept., Colorado State University, Fort Collins, CO*, 2019, p. 69.

[11] Simpson, S., Johns, O., Rose, C., Leckbee, J., Dumitrache, C., Nielsen, D., Yalin, A., and Kiefer, M. "Triggering of a High Pressure Air-Filled High Voltage Spark Gap Switch Using Fiber-Delivered Laser Induced Plasmas Resulting in Sub-Nanosecond Jitter at Low Percentages of Self-Break." *IEEE Pulsed Power Conference*, Vol. Brighton, United Kingdom, 2017, p. 25.

[12] LeChien, K., Savage, M., Anaya, V., Bliss, D., Clark, W., Corley, J., Feltz, G., Garrity, J., Guthrie, D., Hodge, K., Maenchen, J., Maier, R., Prestwich, K., Struve, K., Stygar, W., Thompson, T., Van Den Avyle, J., Wakeland, P., Wallace, Z., and Woodworth, J. "Development of a 5.4 MV Laser Triggered Gas Switch for Multimodule, Multimegampere Pulsed Power Drivers." *Physical Review Special Topics - Accelerators and Beams*, Vol. 11, No. 6, 2008, p. 060402. https://doi.org/10.1103/PhysRevSTAB.11.060402.

[13] Hutsel, B. T., Davis, J.-P., Campbell, R. B., Fowler, W. E., Hanshaw, H. L., Jennings, C., Jones, M., Lemke, R. W., Long, F. W., Lopez, M. R., McKee, G. R., Moore, J. K., Porter, J. L., Savage, M. E., Sceiford, M. E., Stygar, W. A., Corcoran, P. A., Whitney, B. A., Camacho, A. R., Hinshelwood, D., and Wagoner, T. C. Z Machine Circuit Model Development. Presented at the 2013 IEEE 40th International Conference on Plasma Sciences (ICOPS), San Francisco, CA, USA, 2013.

[14] Glover, S. F., Alexander, J. A., Reed, K. W., Pena, G. E., Horry, M. L., Usher, J. M., and Lehr, J. M. "LASER TRIGGERING OF SPARK GAP SWITCHES WITH LESS THAN 100μJ's OF ENERGY." *Sandia National Laboratories*, p. 5.

[15] Carey, W. J., and Mayes, J. R. Marx Generator Design and Performance. Presented at the Conference Record of the Twenty-Fifth International Power Modulator Symposium and 2002 High-Voltage Workshop. International Power Modulator Conference, Hollywood, CA, USA, 2002.

[16] Dzierże˛ga, K., Mendys, A., and Pokrzywka, B. "What Can We Learn about Laser-Induced Plasmas from Thomson Scattering Experiments." *Spectrochimica Acta Part B: Atomic Spectroscopy*, Vol. 98, 2014, pp. 76–86. https://doi.org/10.1016/j.sab.2014.03.010.

[17] Gottfried, J. A., Roux, M., and Yalin, A. P. "Electron Density and Temperature Measurements by Thomson Scattering in a High-Voltage Laser-Triggered Switch." *AIAA Aviation 2022 Forum*, 2022, p. 14. https://doi.org/10.2514/6.2022-3496.

[18] Rose, C., Patel, S. G., Simpson, S., and Yalin, A. P. Preliminary Schlieren and Optical Emission Diagnostics of a High-Voltage Laser Triggered Switch. Presented at the AIAA Aviation 2019 Forum, Dallas, Texas, 2019.

[19] Martin, T. H., Seamen, J. F., and Jobe, D. O. ENERGY LOSSES IN SWITCHES. Presented at the Ninth IEEE International Pulsed Power Conference, Albuquerque, NM, USA, 1993.

[20] Braginskii, S. "Theory of the Development of a Spark Chennel." *J. Exptl. Throret. Phys.*, Vol. 34, Nos. 1548–1557, 1958.

[21] Lavrinovich, I. V., and Oreshkin, V. I. "Numerical Simulation and Analysis of Energy Loss in a Nanosecond Spark Gap Switch." *Journal of Physics: Conference Series*, Vol. 552, 2014, p. 012021. https://doi.org/10.1088/1742-6596/552/1/012021.

[22] Gottfried, J., Rose, C., Simpson, S., and Yalin, A. "Thomson Scattering Measurement of Plasma Evolution During the Current Pulse in a Laser-Triggered Switch." *Under Review*.

[23] Spielman, R. B., Froula, D. H., Brent, G., Campbell, E. M., Reisman, D. B., Savage, M. E., Shoup, M. J., Stygar, W. A., and Wisher, M. L. "Conceptual Design of a 15-TW Pulsed-Power Accelerator for High-Energy-Density–Physics Experiments." *Matter and Radiation at Extremes*, Vol. 2, No. 4, 2017, pp. 204–223. https://doi.org/10.1016/j.mre.2017.05.002.

[24] Beverly, R. E., and Campbell, R. N. "Aqueous-electrolyte Resistors for Pulsed Power Applications." *Review of Scientific Instruments*, Vol. 66, No. 12, 1995, pp. 5625–5629. https://doi.org/10.1063/1.1146029.

[25] Hatae, T., Nagashima, A., Kondoh, T., Kitamura, S., Kashiwabara, T., Yoshida, H., Naito, O., Shimizu, K., Yamashita, O., and Sakuma, T. "YAG Laser Thomson Scattering Diagnostic on the JT-60U." *Review of Scientific Instruments*, Vol. 70, No. 1, 1999, pp. 772–775. https://doi.org/10.1063/1.1149392.

[26] Dzierżęga, K., Mendys, A., Pellerin, S., Thouin, E., Travaille, G., Bousquet, B., Canioni, L., and Pokrzywka, B. Thomson Scattering from Laser Induced Plasma in Air. J. Phys.: Conf. Ser. 227 012029, , 2010.

[27] Murray, C. S. "Evolution of Electron Properties After Nanosecond Repetitively Pulsed Discharges in Air Measured by Thomson Scattering." *M.Sc. Thesis, Physics Dept., Wright State University, Dayton, OH*, 2020, p. 68.

[28] Sande, M. van de, and Sande, M. J. van de. *Laser Scattering on Low Temperature Plasmas: High Resolution and Stray Light Rejection*. 2002.

[29] Ross, J. S., Glenzer, S. H., Palastro, J. P., Pollock, B. B., Price, D., Tynan, G. R., and Froula, D. H. "Thomson-Scattering Measurements in the Collective and Noncollective Regimes in Laser Produced Plasmas (Invited)." *Review of Scientific Instruments*, Vol. 81, No. 10, 2010, p. 10D523. https://doi.org/10.1063/1.3478975.

[30] Suttle, L. G., Hare, J. D., Halliday, J. W. D., Merlini, S., Russell, D. R., Tubman, E. R., Valenzuela-Villaseca, V., Rozmus, W., Bruulsema, C., and Lebedev, S. V. "Collective Optical Thomson Scattering in Pulsed-Power Driven High Energy Density Physics Experiments (Invited)." *Review of Scientific Instruments*, Vol. 92, No. 3, 2021, p. 033542. https://doi.org/10.1063/5.0041118.

[31] Tomita, K., Kagawa, T., Uchino, K., Katsuki, S., and Akiyama, H. "Collective Thomson Scattering Diagnostics of EUV Plasmas." 2009, p. 5.

[32] Salpeter, E. E. "Electron Density Fluctuations in a Plasma." *Physical Review*, Vol. 120, 1960, pp. 1528–1535. https://doi.org/doi:10.1103/physrev.120.1528.

[33] Friss, A. J. "CAVITY ENHANCED THOMSON SCATTERING FOR PLASMA DIAGNOSTICS." *Ph.D. Dissertation, Mechanical Engineering Dept., Colorado State University, Fort Collins, CO*, 2019, p. 183.

[34] Hutchinson, I. H. *Principles of Plasma Diagnostics*. Cambridge University Press, 2002.

[35] Fried, B. D., and Conte, S. D. TABLE GENERATION AND ACCURACY. In *The Plasma Dispersion Function*, Elsevier, 1961, pp. 5–7.

[36] Savage, M. Pulsed Power Electrical Diagnostics Techniques and Analysis. IEEE Pulsed Power-Plasma Science Mini-course, Jun 23, 2007.

[37] Spitzer, L., and Härm, R. "Transport Phenomena in a Completely Ionized Gas." *Physical Review*, Vol. 89, No. 5, 1953, pp. 977–981. https://doi.org/10.1103/PhysRev.89.977.

[38] Shah, S. I. W. "VARIATION OF PLASMA RESISTIVITY DURING TOKAMAK START-UP." p. 7.

[39] Honda, M. “Coulomb Logarithm Formulae for Collisions between Species with Different Temperatures.” *Japanese Journal of Applied Physics*, Vol. 52, No. 10R, 2013, p. 108002. https://doi.org/10.7567/JJAP.52.108002.
[40] Chen, F. F. *Introduction to Plasma Physics and Controlled Fusion*. Springer International Publishing, Cham, 2016.
[41] Weber, R. E., and Tempelmeyer, K. E. *CALCULATION OF THE D-C ELECTRICAL CONDUCTIVITY OF EQUILIBRIUM NITROGEN AND ARGON PLASMA WITH AND WITHOUT ALKALI METAL SEED:* Defense Technical Information Center, Fort Belvoir, VA, 1964.
[42] Cohen, R. S., Spitzer, L., and Routly, P. McR. “The Electrical Conductivity of an Ionized Gas.” *Physical Review*, Vol. 80, No. 2, 1950, pp. 230–238. https://doi.org/10.1103/PhysRev.80.230.
[43] Trintchouk, F., Yamada, M., Ji, H., Kulsrud, R., and Carter, T. “Measurement of the Transverse Spitzer Resistivity during Collisional Magnetic Reconnection.” *Princeton Plasma Physics Laboratory*, 2002.